Jurnal Teknologi

Full Paper

TAGUCHI OPTIMIZATION OF X70 CARBON STEEL HEAT TREATMENT: A STUDY ON HARDNESS, THICKNESS AND PHASE ANALYSIS

Umi Zalilah, Dharmesh Kumar, Skandha Kumar, Mazli Mustapha*

Mechanical Engineering Department, Universiti Teknologi PETRONAS, 32610, Seri Iskandar, Perak, Malaysia

Article history
Received
19 September 2024
Received in revised form
16 December 2024
Accepted
16 December 2024
Published Online
22 August 2025

*Corresponding author
mazli.mustapha@utp.edu.my

Graphical abstract

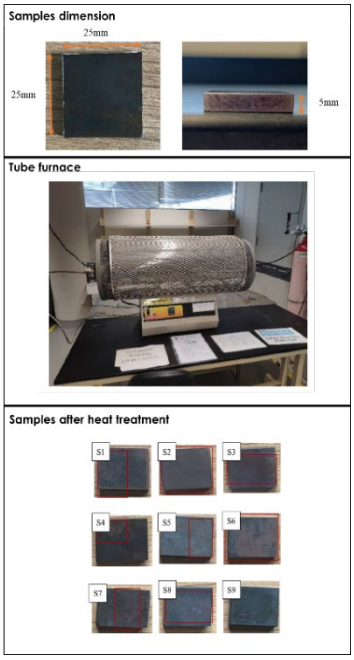

Abstract

The application of carbon steel fiber metal laminate (CFML) has been increasing in engineering industries such as aerospace, automotive and processing industries. In fabricating CFML, the surface quality is a fundamental criterion as its stability is the key to avoiding delamination and corrosion. Delamination and corrosion can be prevented by growing a fresh and stable oxide layer with good mechanical properties via heat treatment on carbon steel. In this paper, the influence of heat treatment parameters namely temperature (400, 600 and 800 ^{0}C), heating time (60, 90 and 120 min), heating rate (10, 15 and 20 ^{0}C/min) and substrate roughness (P80, P240 and P800) on the X70 carbon steel oxide phase formation, thickness and hardness properties were investigated. Using Taguchi's method, a total of 9 experiments were performed based on the L9 orthogonal array. The signal-to-noise ratio (S/N) and contribution percentage of the analysis of variance (ANOVA) of each parameter on the responses were studied. The optimal conditions for thickness were obtained at temperature 800 ºC, heating time 120mins, heating rate 10 ºC/min and sample prepared with P80 sandpaper grit. Meanwhile, optimal conditions for hardness were obtained at temperature 800 ºC, heating time 120mins, heating rate 10 ºC/min and sample prepared with P80 sandpaper grit.

Keywords: Pipeline steel, Heat treatment, Iron oxide, Phase analysis, Carbon Fiber Metal Laminate

Abstrak

Penggunaan gentian logam pada keluli karbon (CFML) semakin meningkat dalam industri seperti dalam sektor aeronangkasa, automotif dan pemprosesan. Kualiti permukaan keluli karbon adalah kriteria asas kepada kestabilan CFML bagi menghindari dari delaminasi dan kakisan. Delaminasi dan kakisan boleh dicegah dengan cara membina satu lapisan oksida yang stabil bersama dengan sifat mekanikal yang bagus pada permukaan keluli karbon melalui rawatan haba. Dalam kertas kerja ini, pengaruh faktor rawatan haba iaitu suhu (400, 600 dan 800 ^{0}C), masa pemanasan (60, 90 dan 120 min), kadar pemanasan (10, 15 dan 20 ^{0}C/min) dan kekasaran substrat (P80, P240 dan P800) pada pembentukan lapisan oksida, sifat ketebalan dan kekerasannya telah dikaji. Kaedah Taguchi telah digunakan iaitu sebanyak 9 eksperimen telah dilakukan berdasarkan tatasusunan ortogon L9. Nisbah isyarat-kepada-bunyi (S/N) dan peratusan sumbangan analisis varians (ANOVA) bagi setiap faktor pada tindak balas telah dikaji. Keadaan optimum untuk ketebalan diperolehi pada suhu 800 ºC, masa pemanasan 120minit, kadar pemanasan 10 ºC/min dan sampel yang disediakan dengan kertas pasir grit P80. Sementara itu, keadaan optimum untuk kekerasan diperoleh pada suhu 800 ºC, masa pemanasan 120minit, kadar pemanasan 10 ºC/min dan sampel yang disediakan dengan kertas pasir grit P80.

Kata kunci: Keluli saluran paip, Rawatan haba, Oksida besi, Analisis fasa, Laminasi logam gentian karbon.

1.0 INTRODUCTION

Carbon steel (hereafter referred to as CS) is undoubtedly the most useful engineering material that has been used in various industries like petroleum (transporting oil, gas and other media), chemical (pressure vessels and piping systems), electric power fields (as boilers, chimneys) and construction fields (water supply, drainage and heating) [1, 2, 3, 4]. Typically, X70 and X80 are used in major projects all over the world with thicknesses varying between 15 mm to 22 mm. They are known to be the most often used steel for pipeline construction because they are economical, affordable and long lasting. The main characteristics of CS include high strength, high yield strength, high tensile strength, good hardness and toughness. However, despite its good mechanical qualities, the CS is still prone to corrosion. Corrosion happens when oxygen and water vapor that are available in the aqueous environment react with the iron element of CS producing iron oxide i.e. rust. This occurrence consumes iron elements in the CS making material to reduce and corrode hence shortening the life of the pipeline system [5, 6].

The introduction of composites including fiber metal laminate (FML) has become revolutionary in remediating corrosion thus increasing the lifespan of industrial pipelines [7, 8]. FML is a hybrid composite structure formed by interlacing metal layers with fiber reinforced plastics such as fiber glass and carbon fibers. The fibers in the FML protect the metal from corrosion while at the same time providing excellent stiffness, fatigue and strength [9], [10, 11]. Carbon fiber metal laminate (CFML) is a common fiber laminate that has been widely used as protection for the corrosion problem in industrial pipelines [12, 13, 14]. In the fabrication of CFML structures, CS surface quality plays an important role because it can affect the bonding with the FML. Corrosion and reduction on the CS surface can disrupt the bonding between CS and FML which can lead to the delamination phenomenon[15 ,16]. Nevertheless, the corrosion and delamination probability of the CFML can be reduced by growing a fresh and stable oxide layer on the CS. This is because the grown oxide layer acts as passivation on the CS which protects it from further corrosion while also improving the adhesion between the steel and epoxy network [17], [18]. From the available literature, there is limited research that studies the influence of heat treatment parameters on the oxide phase stability as well as lack of optimal guidelines for CFML applications. Hence this study aims to fill that gap [19, 20].

Iron oxides formed on the CS can be hematite (Fe_2O_3), magnetite (Fe_3O_4) and wustite (FeO). Hematite, generally known as rust, forms at normal oxidizing conditions regardless of pH, is less stable and porous and is very reactive at high oxygen concentrations, which speeds up the corrosion process. The formation of hematite in the presence of oxygen in moist air can be represented by:

$$4Fe + 3O_2 \rightarrow 2Fe_2O_3Fe \qquad \ldots (1)$$

Unlike hematite, magnetite (Fe_3O_4) is a stable compound that is able to passivate the CS surface. In other words, magnetite can act as CS protection from corrosion. The chemical equation for magnetite formation can be represented by:

$$Fe + 4Fe_2O_3 \leftrightarrow Fe_3O_4Fe \qquad \ldots (2)$$

In marine applications, magnetite-epoxy nanocomposite has been used as a protective coating as the damaged epoxy layer compromises with magnetite and heals the cracks [21]. It has also been shown that the adhesion between the epoxy and steel network improved as the magnetite content increased. Another possible oxide form on the CS is wustite (FeO). Wustite displays good stability at temperatures higher than 570 ^{0}C. At low temperatures, wustite breaks down into magnetite and iron as a chemical equation as follows:

$$4FeO \rightarrow Fe_3O_4 + Fe \qquad \ldots (3)$$

Among the oxides, magnetite is the preferred oxide to be grown on the CS as it's the most stable and can serve as a protection layer. The formation of magnetite on CS can be controlled by controlling the heat treatment parameters, namely temperature, heating time, heating rate and CS surface roughness. Temperature is one of the fundamental parameters that can affect the oxide formation as well as the wustite, magnetite and hematite proportions [22], [23]. Meanwhile, heating time works cohesively with temperature as at certain durations and temperatures, different oxides are formed. Besides, different exposure durations of CS at high temperatures will result in different oxide layer thicknesses [24, 25].

The heating rate can influence the oxide formation as it can affect the oxidation rate. Despite that, a high heating rate may also cause unstable oxide growth. Lastly, there is roughness on the surface. Different roughness levels on the CS surface can be achieved by grinding the samples with different grit papers. This method was also used to remove any undesirable natural passive oxide layer in the early stages. The physico-chemical changes from the mechanical abrasion treatment are able to yield a wettable surface and modify the surface topography [26, 27]. Then, heat treatment with proper parameters will cover the CS with a fresh, stable oxide layer with a desirable chemical composition. To understand the effect of various heat treatment parameters on the iron oxide phase formation and its consequences on the mechanical properties, the Taguchi method was utilized to design the experiment. The Taguchi method is a well-known optimization and statistical tool used in ranking the importance of different factors for a target function which allows a smaller number of experiments because it uses an orthogonal array to minimize the effects of noise factors. Additionally, the Taguchi method examines the performance of the parameters using the signal-to-noise (S/N) ratio and

analysis of variance (ANOVA) [28, 29]. In this research, heat treatment was used to grow oxide layers on CS samples. Taguchi optimization method was utilized to design the experiment involving temperature, heating time, heating rate and surface roughness parameters. The objective is to investigate the effect of heat treatment parameters on the oxide layer hardness, thickness and phase formation.

2.0 METHODOLOGY

In the present study, CS X70 grade was used, and its chemical composition is given in Table 1.

Table 1 Chemical composition of the API X70 steel (wt.%)

C	Si	Mn	S	P	
0.061	0.24	1.53	0.0009	0.011	
Cr	Ni	Mo	Nb	Cu	Fe
0.024	0.21	0.23	0.038	0.01	Remaining

The raw material was cut using a precision cutter into 25 x 25 x 5 mm dimensions. The parameters investigated in this study were temperature, heating rate, heating time and sample surface roughness which was chosen were based on preliminary studies that had been done prior. Different surface roughness on the samples were achieved by grinding the samples with different sandpaper grits (P80, P240 and P800). The higher sandpaper grit, the finer abrasive particles, hence producing smoother surfaces. The surface roughness of the grounded samples was confirmed using Mitutoyo Surftest surface roughness tester. Multiple scans were taken in several areas of each sample with averages calculated. The surface roughness obtained for samples prepared by P80, P240 and P800 sandpapers grit were 1.37µm, 0.95µm and 0.19µm respectively. Samples were then placed into the tube furnace where heat was supplied with atmospheric conditions. Parameters like temperature, heating rate and heating time were set according to the Taguchi L9 orthogonal array design matrix as tabulated in Table 2 and Table 3.

Once heat treatment was done, samples were taken out of the furnace and kept in a normal ambient environment to be cooled over time. The thickness and elemental analysis present on the samples were investigated using the Hitachi TM3000 scanning electron microscope (SEM) equipped with Quantax70 electron spectroscopy (EDS) analysis. Meanwhile, phases presents were identified using XRD Malvern Panalytical X' Pert. The XRD diffractometer was set to 40kV, 40mA at room temperature with Cu-Ka radiation (k = 1.54060 Å) in the range $2\theta = 5^0 \sim 80^0$. The hardness of the treated samples was measured using LECO LM247 AT micro-hardness Vickers tester following the ASTM E384 standard. Taguchi and ANOVA analyses from the Minitab19 statistical software were utilized to analyze the effect of heat treatment parameters on thickness and hardness values. The correlation between phases obtained with the heat treatment parameters as well as the mechanical properties of the samples were discussed.

Table 2 Process parameters and level for value L^9 (3_4) orthogonal array design matrix

Parameter	Level 1	Level 2	Level 3
Temperature	400	600	800
Time	60	90	120
Heating Rate	10	15	20
Surface Roughness (grit sandpapers)	P80	P240	P800

Table 3 Experimental design

Exp No.	Setup Label	Process parameter			
		Temperature (^{0}C)	Time (min)	Heating rate (^{0}C/min)	Surface roughness (grit sandpaper)
1	S1	400	60	10	P80
2	S2	400	90	15	P240
3	S3	400	120	20	P800
4	S4	600	60	15	P800
5	S5	600	90	20	P80
6	S6	600	120	10	P240
7	S7	800	60	20	P240
8	S8	800	90	10	P800
9	S9	800	120	15	P80

3.0 RESULTS AND DISCUSSION

3.1 Phase investigations

The phases present at each experiment setup were investigated via XRD. The diffractograms of S1 until S9 were illustrated in Figure 1. It can be observed that from S1 until S4, the samples were composed of magnetite peaks with the highest intensity at position 45^0. A few low intensity magnetite peaks can also be observed at positions 33.1^0, 35.5^0, 43.0^0 and 65.0^0. Low intensity hematite compound peaks were detected in the background, while no wustite phase peaks were visible from S1 until S3. The trend for increasing magnetite intensity peaks starting from S1 until it reaches the highest intensity at S4. Starting from S5 onwards, magnetite peaks become less with low intensity until they reach the lowest at S9. Opposite to the magnetite peaks trend that becoming less from S5 to S9, hematite low intensity peaks that exist in the background at the beginning have become more visible from S5 onwards. Hematite phases showed the most peak counts with the highest intensity at S5. As for the wustite phase, it exists at low intensity for samples prepared with S8 and S9 setups. No wustite phases can be observed at other setups. Referring to the FeO equilibrium phase diagram in Figure 2, the

absence of wustite can be due to its amount being too small or its decomposition into magnetite and aFe. The thermodynamic instability of wustite phases at low temperatures can also be found in [30, 31, 32] findings.

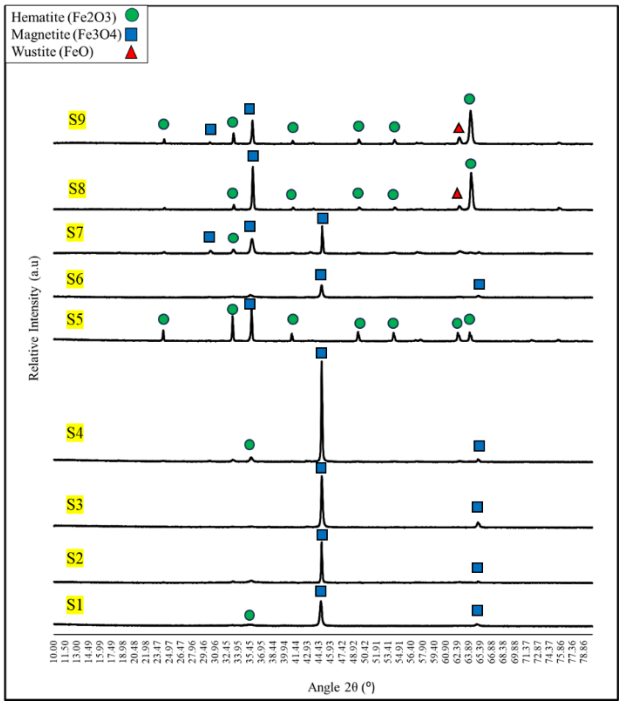

Figure 1 XRD diffractogram of S1, S2, S3, S4, S5, S6, S7, S8 and S9 experiments

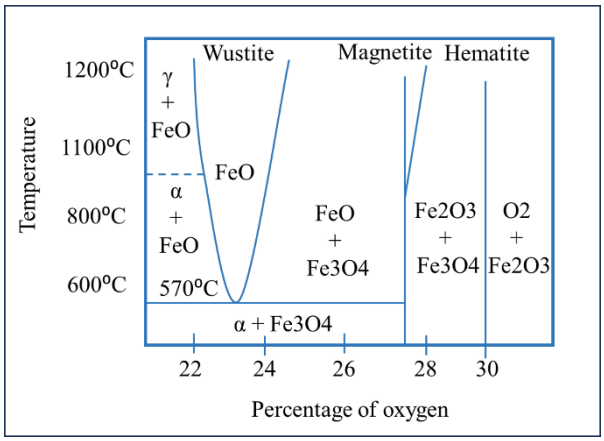

Figure 2 FeO phase diagram [22].

The transition from magnetite as the main peaks (S1 to S4) to hematite as the major peaks (S5 onwards) can be related to redox reactions [33]. Magnetite oxidation is mainly affected by temperature, such that the oxidation of magnetite to hematite at room temperature is not possible. In the present study results, it was inferred that at lower temperatures the reaction rate is slow thus making the major phase exist as magnetite. Only by heating the samples to more than 600^{0}C, does the magnetite crystalline structure change hence the transition to the hematite phase occurs. From the phase investigations, the phases formed and transitions were as expected in accordance with the phase diagram as well as aligned with other researchers findings [34, 35, 36].

3.2 Oxide Layer Thickness

Using the Taguchi and ANOVA analyses, the impact of heat treatment parameters on the thickness of the CS oxide layer was examined. According to Canbolat (2019), the design parameters with maximum S/N ratios indicate the optimum conditions of the system. Moreover, if the highest and lowest S/N ratio variations are small, it implies that there is a relatively low effect of the parameters on the response. According to Figure 4 (b), S/N ratio analysis for oxide layer thicknesses showed that temperature was the parameter that had the biggest impact on the oxide layer thickness results, followed closely by the heating time parameter. Meanwhile, heating rate and surface roughness come next. For the results to be statistically reliable, the ANOVA method was used to validate the Taguchi results. Figure 4 (c) of the ANOVA results showed that temperature contributes 64.0% to the oxide layer thickness, followed by heating time (28.1%), heating rate (5.0%) and surface roughness (2.9%). This ANOVA analysis result showed the same trend as the Taguchi analysis thus validating the results. Figure 3 visualizes the SEM micrograph of oxide layer thickness samples for S7, S8 and S9 where these samples were prepared at the same temperature (800^{0}C) but with different heating times. The effect of temperature on the oxide layer thickness can be seen more clearly from S8 to S9, where the oxide layer thickness increases significantly from 57.17 µm to 121.32 µm. Please note that the delamination observed in samples was due to the sample preparation process (cutting, grinding and polishing process) for SEM observations. According to the kinetic reaction of the parabolic law, at high temperatures, magnetite phases were further transformed into hematite phases which can be seen from the XRD diffraction pattern. Following this transformation, the density of the starting material will keep falling while the weight of the oxide as well as the thickness will increase due to more oxygen being taken up [38, 39]. The second factor contributing to the oxide layer thickness as per S/N ratio and ANOVA analysis was the heating time. It can be observed from Figure 4 (a), that samples prepared under the same heating time but at different heating temperatures (S2, S4 and S7) showed a steady increase in oxide layer thickness. A longer heating time allows more reaction and diffusion to happen on the CS thus resulting in a thicker oxide layer.

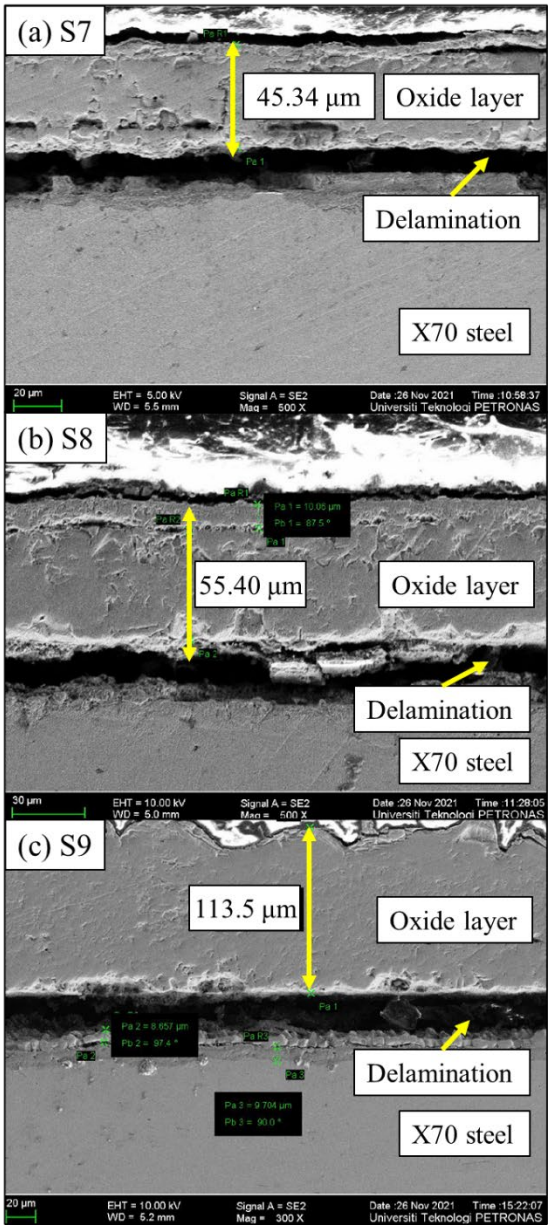

Figure 3 SEM micrograph of S7, S8 and S9 setups

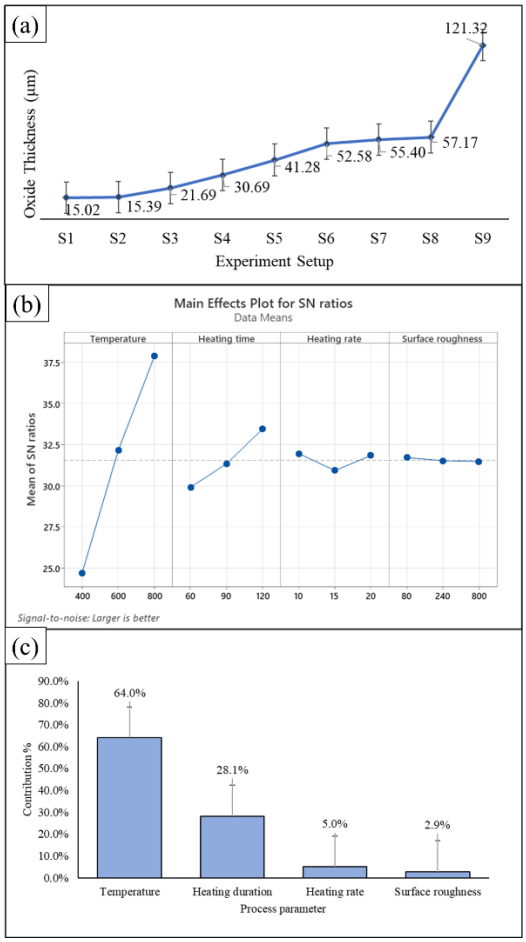

Figure 4 (a) Oxide layer thickness for all experiment setups, (b) S/N ratio and (c) contributions percentage of heat treatment parameters on the oxide layer thickness responses

3.3 Hardness Measurement

Figure 5 (a) represents the average hardness values obtained from all the experiment's setups. It can be observed that the highest hardness values were obtained from S9, followed by S5, S6, S1, S8, S7, S4, S2 and S3. These hardness results were further investigated using the S/N ratio and ANOVA analysis to understand the influence and contribution of each heat treatment parameter on the hardness values. Figure 5 (b) and (c) present the S/N ratios result and ANOVA contribution percentage on the hardness value response. Both analyses showed the same trend, whereby the main factor impacting the hardness value was surface roughness with a contribution percentage of 60.1% followed by temperature (32%), heating time (4%) and heating rate (3%). Bresson (2012) reported that excessive roughness could have a negative influence on the bonding strength due to its ability to decrease adhesive resin penetration, increase void formation and introduce localized stress concentration. This argument contradict with Rudawska (2016), which suggested that increasing the surface roughness of

the substrate could enhance the bonding strength. In the present study, samples prepared using P80 grit which is the lowest grit paper producing a rougher surface have the highest hardness value. This can be due to the CS rougher surface helping to enhance the oxide layer bonding strength. The hardness value results can also be correlated with phases observed in the XRD diffractogram. The highest hardness values were obtained at the S9 setup, whereby this setup showed hematite as the main peak in the diffractogram. As is known, among the iron oxide phases, hematite possessed the highest hardness, followed by magnetite and then wustite. Thus, given that the S9 setup exhibits high counts and intensity of hematite phases resulting in a high hardness value. Inversely, setup with magnetite as the main phase exhibits a lower hardness value compared to setup with hematite as the main phase. The hardness obtained in relation to each oxide were aligned with those of the individual iron oxides (FeO, Fe_3O_4 and Fe_2O_3) reported in the literatures [42, 43, 44]. The small difference of values in this study with the literatures could be attributed to the variations in the wustite, magnetite and hematite proportions in each oxide as well as the methods used to determine the hardness.

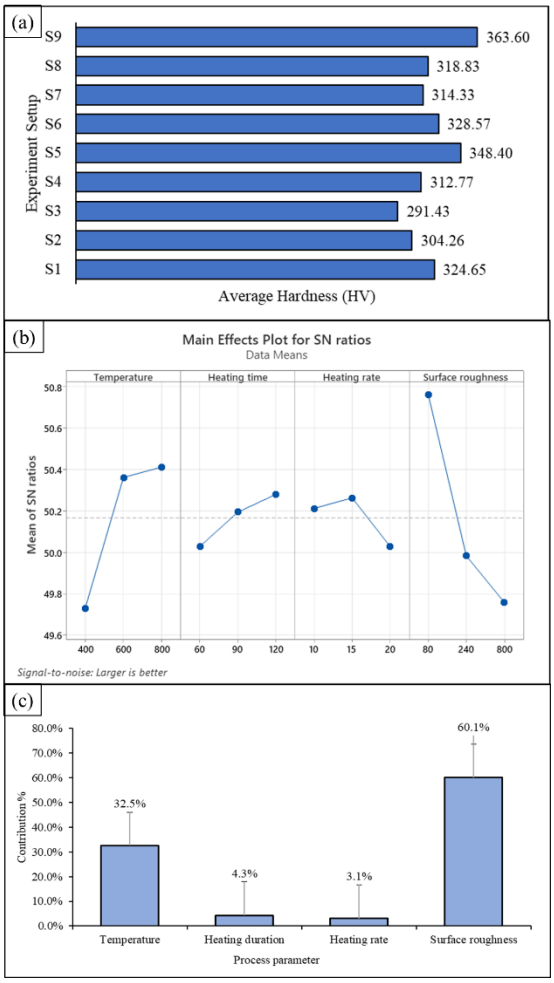

Figure 5 (a) Hardness value for all experiment setup, (b) S/N ratio and (c) contribution percentage of heat treatment parameters on the hardness value responses

4.0 CONCLUSION

In this study, an L9 orthogonal array was used to study the effect of tube furnace heat treatment parameters on phase formation, oxide layer thickness and hardness properties. The Taguchi method and ANOVA analyses were utilized to understand every parameter's impact on the response properties. It can be concluded that temperature is the main parameter that affects the phase of the oxide layer. The preferrable stable magnetite phase was able to grow at temperature below 600^{0}C but it is not high enough to transform it into hematite phase. Meanwhile, at this temperature, wustite phase was thermodynamically unstable hence prone to decompose into magnetite and iron phase. The oxide layer thickness formation was mainly affected by the parameters with the optimum condition maximizing the oxide layer were as follows temperature (800^{0}C), heating time(120mins), heating rate (10 ^{0}C/min) and surface roughness (prepared with P80 sandpaper grit). The hardness value was mainly affected by the parameters with the optimum condition maximizing the hardness were as follows temperature (800 ^{0}C), heating time (120mins), heating rate (15 ^{0}C/min) and surface roughness (prepared with P80 sandpaper grit). Future studies could be considered the effect of process parameters on the properties and performance of X70 carbon steel under sour corrosive environment which has always been a concern for the oil and gas exploration industries. Aside, laminated heat-treated samples with CFML also can be done to study their compatibility and durability.

Acknowledgement

This research is supported by the Yayasan Universiti Teknologi PETRONAS via YUTP-FRG 015LC0- 474 grant. The authors also would like to thank Universiti Teknologi PETRONAS (UTP) for providing resources to perform this research.

Conflicts of Interest

The authors declare that there is no conflict of interest regarding the publication of this paper.

References

[1] H. Karampour, M. Alrsai, F. Albermani, H. Guan, and D.-S. Jeng. 2017. Propagation Buckling in Subsea Pipe-in-Pipe Systems. *J. Eng. Mech.* 143(9): 04017113. Doi: 10.1061/(ASCE)EM.1943-7889.0001337.

[2] G. P. Drumond, I. P. Pasqualino, B. C. Pinheiro, and S. F. Estefen. 2018. Pipelines, Risers and Umbilicals Failures: A Literature Review. *Ocean Engineering*. 148: 412–425. Doi: 10.1016/j.oceaneng.2017.11.035.

[3] M. S. Egene, O. Adedipe, U. G. Okoro, and K. T. Obanimomo. 2021. Investigation of Fracture Behaviour of

API X70 Pipeline Steel. *IOP Conf. Ser.: Mater. Sci. Eng.* 1107(1): 012184. Doi: 10.1088/1757-899X/1107/1/012184.
[4] E. Arzaghi, B. H. Chia, M. M. Abaei, R. Abbassi, and V. Garaniya. 2020. Pitting Corrosion Modelling of X80 Steel Utilized in Offshore Petroleum Pipelines. *Process Safety and Environmental Protection*. 141: 135–139. Doi: 10.1016/j.psep.2020.05.024.
[5] G. Yang *et al.* 2024. Effect of Dissolved Oxygen on Corrosion Behavior and Mechanism of X70 Pipeline Steel in Simulated Low Temperature Bentonite-containing Alkaline Chloride Environment. *Construction and Building Materials*. 438: 137170. Doi: 10.1016/j.conbuildmat.2024.137170.
[6] T. T. Nguyen, H. M. Heo, J. Park, S. H. Nahm, and U. B. Beak. 2021. Fracture Properties and Fatigue Life Assessment of API X70 Pipeline Steel under the Effect of an Environment Containing Hydrogen. *J Mech Sci Technol*. 35(4): 1445–1455. Doi: 10.1007/s12206-021-0310-0.
[7] F. G. Alabtah, E. Mahdi, and F. F. Eliyan. 2021. The Use of Fiber Reinforced Polymeric Composites in Pipelines: A Review. *Composite Structures*. 276: 114595. Doi: 10.1016/j.compstruct.2021.114595.
[8] A. Saffar, A. Darvizeh, R. Ansari, A. Kazemi, and M. Alitavoli. 2021. Damage Analysis of Fiber–metal Laminate Patches as a Repair System for Surface Defects of Steel Pipelines. *Proceedings of the Institution of Mechanical Engineers, Part L: Journal of Materials: Design and Applications*. 235(4): 868–879. Doi: 10.1177/1464420720980148.
[9] A. Salve, R. Kulkarni, and A. Mache. 2016. A Review: Fiber Metal Laminates (FML's) - Manufacturing, Test Methods and Numerical modeling. *IJETS*. 3(2): 71–84. Doi: 10.15282/ijets.6.2016.1.10.1060.
[10] G. Franz, P. Vantomme, and M. H. Hassan. 2022. A Review on Drilling of Multilayer Fiber-Reinforced Polymer Composites and Aluminum Stacks: Optimization of Strategies for Improving the Drilling Performance of Aerospace Assemblies. *Fibers*. 10(9): 78. Doi: 10.3390/fib10090078.
[11] R. D. F. S. Costa, R. C. M. Sales-Contini, F. J. G. Silva, N. Sebbe, and A. M. P. Jesus. 2023. A Critical Review on Fiber Metal Laminates (FML): From Manufacturing to Sustainable Processing. *Metals*. 13(4): 638. Doi: 10.3390/met13040638.
[12] M. Mokhtari and A. Alavi Nia. 2016. The Application of CFRP to Strengthen Buried Steel Pipelines against Subsurface Explosion. *Soil Dynamics and Earthquake Engineering*. 87: 52–62. Doi: 10.1016/j.soildyn.2016.04.009.
[13] Y. Zhang, Z. Liu, J. Xin, Y. Wang, C. Zhang, and Y. Zhang. 2021. The Attenuation Mechanism of CFRP Repaired Corroded Marine Pipelines based on Experiments and FEM. *Thin-Walled Structures*. 169: 108469. Doi: 10.1016/j.tws.2021.108469.
[14] M. Elchalakani, A. Karrech, H. Basarir, M. F. Hassanein, and S. Fawzia. 2017. CFRP Strengthening and Rehabilitation of Corroded Steel Pipelines under Direct Indentation. *Thin-Walled Structures*. 119: 510–521. Doi: 10.1016/j.tws.2017.06.013.
[15] B. Surowska, P. Jakubczak, and J. Bieniaś. 2017. Structure and Chemistry of Fiber Metal Laminates. *Hybrid Polymer Composite Materials*. 193–234. Doi: 10.1016/B978-0-08-100791-4.00008-2.
[16] M. Droździel-Jurkiewicz and J. Bieniaś. 2022. Evaluation of Surface Treatment for Enhancing Adhesion at the Metal–Composite Interface in Fibre Metal-Laminates. *Materials*. 15(17): 6118. Doi: 10.3390/ma15176118.
[17] Marcus, P and Oudar,J. 2022. *Corrosion Mechanisms in Theory and Practice*. New York: Marcel Dekker.
[18] Y. Wang, X. Liu, H. Wang, and K. Vecchio. 2020. The Effect of Oxides on Fe/Al interfacial Reaction in Metal-Intermetallic Laminate (MIL) Composites. *Journal of Alloys and Compounds*. 845: 156268. Doi: 10.1016/j.jallcom.2020.156268.
[19] Y. Saito, H. Watanabe, T. Yamada, K. Kanamori, and A. Yonezu. 2019. Interfacial Strength Evaluation of Oxide Films on Carbon Steel by Using the Laser Shock Adhesion Test. *J. of Materi Eng and Perform*. 28(8): 4762–4773. Doi: 10.1007/s11665-019-04246-1.
[20] B. Fayzulla, M. Eroglu, and I. Qader. 2023. Multifunctional Properties of Metal Fibers Reinforced Polymer Composites ndash; A Review. *MACS*. Online First. Doi: 10.22075/macs.2023.29308.1461.
[21] A. M. Atta, A. M. El-Saeed, G. M. El-Mahdy, and H. A. Al-Lohedan. 2015. Application of Magnetite Nano-hybrid Epoxy as Protective Marine Coatings for Steel. *RSC Adv.* 5(123): 101923–101931. Doi: 10.1039/C5RA20730D.
[22] W. Sun, A. K. Tieu, Z. Jiang, H. Zhu, and C. Lu. 2004. Oxide Scales Growth of Low-carbon Steel at High Temperatures. *Journal of Materials Processing Technology*. 155–156: 1300–1306. Doi: 10.1016/j.jmatprotec.2004.04.172.
[23] J. S. Sheasby, W. E. Boggs, and E. T. Turkdogan. 1984. Scale Growth on Steels at 1200°C: Rationale of Rate and Morphology. *Metal Science*. 18(3): 127–136. Doi: 10.1179/msc.1984.18.3.127.
[24] F. S. Ahmed, M. A. El-Zomor, M. S. A. Ghazala, and R. N. Elshaer. 2022. Effect of Oxide Layers Formed by Thermal Oxidation on Mechanical Properties and NaCl-induced Hot Corrosion Behavior of TC21 Ti-alloy. *Sci Rep*. 12(1): 19265. Doi: 10.1038/s41598-022-23724-6.
[25] M. O. Carvalho, L. A. Matlakhova, S. N. Monteiro, R. S. T. Manhães, and N. A. Palii. 2024. Analysis of Oxide Layer Formation During Oxidation of AISI 4140 Steel at 1000 °C over Exposure Time. *Metals*. 14(11): 1251. Doi: 10.3390/met14111251.
[26] S. Y. Park, W. J. Choi, H. S. Choi, H. Kwon, and S. H. Kim. 2010. Recent Trends in Surface Treatment Technologies for Airframe Adhesive Bonding Processing: A Review (1995–2008). *The Journal of Adhesion*. 86,(2): 192–221. Doi: 10.1080/00218460903418345.
[27] A. F. Harris and A. Beevers. 1999. The Effects of Grit-blasting on Surface Properties for Adhesion. *International Journal of Adhesion and Adhesives*. 19(6): 445–452. Doi: 10.1016/S0143-7496(98)00061-X.
[28] G. Taguchi and S. Konishi. 1987. *Taguchi Methods: Orthogonal Arrays and Linear Graphs; Tools for Quality Engineering*. American Supplier Institute.
[29] O. O. Agboola *et al.* 2020. Optimization of Heat Treatment Parameters of Medium Carbon Steel Quenched in Different Media using Taguchi Method and Grey Relational Analysis. *Heliyon*. 6(7). Doi: 10.1016/j.heliyon.2020.e04444.
[30] Z. Zhang. 2023. The Characteristics and Reduction of Wustite. *Iron Ores and Iron Oxides - New Perspectives*, B. Kumar, Ed. IntechOpen. Doi: 10.5772/intechopen.1001051.
[31] R. Nisticò. 2021. A Synthetic Guide Toward the Tailored Production of Magnetic Iron Oxide Nanoparticles. *Boletín de la Sociedad Española de Cerámica y Vidrio*. 60(1): 29–40. Doi: 10.1016/j.bsecv.2020.01.011.
[32] S.-N. Lin, C.-C. Huang, M.-T. Wu, W.-L. Wang, and K.-C. Hsieh. 2017. Crucial Mechanism to the Eutectoid Transformation of Wüstite Scale on Low Carbon Steel. Doi: 10.20944/preprints201701.0130.v1.
[33] Z. Li, C. Chanéac, G. Berger, S. Delaunay, A. Graff, and G. Lefèvre. 2019. Mechanism and Kinetics of Magnetite Oxidation under Hydrothermal Conditions. *RSC Adv.* 9(58): 33633–33642. Doi: 10.1039/C9RA03234G.
[34] R. Y. Chen. 2003. Review of the High-Temperature Oxidation of Iron and Carbon Steels in Air or Oxygen. *Oxidation of Metals*. 59(5/6): 433–468. Doi: 10.1023/A:1023685905159.
[35] S. Nasrazadani and A. Raman. 1993. The Application of Infrared Spectroscopy to the Study of Rust Systems—II. Study of Cation Deficiency in Magnetite (Fe_3O_4) Produced during its Transformation to Maghemite (γ-Fe_2O_3) and Hematite (α-Fe_2O_3). *Corrosion Science*. 34(8): 1355–1365. Doi: 10.1016/0010-938X(93)90092-U.
[36] H. Lepp. 1957. Stages in the Oxidation of Magnetite. *American Mineralogist*. 42(9–10): 679–681.
[37] A. S. Canbolat, A. H. Bademlioglu, N. Arslanoglu, and O. Kaynakli. 2019. Performance Optimization of Absorption Refrigeration Systems using Taguchi, ANOVA and Grey

Relational Analysis Methods. *Journal of Cleaner Production*. 229: 874–885. Doi: 10.1016/j.jclepro.2019.05.020.
[38] D. J. Young. 2016. *High Temperature Oxidation and Corrosion of Metals*. Elsevier. Doi: 10.1016/c2014-0-00259-6.
[39] S. A. Arreola-Villa, H. J. Vergara-Hernández, G. Solorio-Diáz, A. Pérez-Alvarado, O. Vázquez-Gómez, and G. M. Chávez-Campos. 2022. Kinetic Study of Oxide Growth at High Temperature in Low Carbon Steel. *Metals*. 12(1): 147. Doi: 10.3390/met12010147.
[40] G. Bresson, J. Jumel, M. E. R. Shanahan, and P. Serin. 2012. Strength of Adhesively Bonded Joints under Mixed Axial and Shear Loading. *International Journal of Adhesion and Adhesives*. 35: 27–35. Doi: 10.1016/j.ijadhadh.2011.12.006.
[41] A. Rudawska, I. Danczak, M. Müller, and P. Valasek. 2016. The Effect of Sandblasting on Surface Properties for Adhesion. *International Journal of Adhesion and Adhesives*. 70: 176–190. Doi: 10.1016/j.ijadhadh.2016.06.010.
[42] O. A. Zambrano, J. J. Coronado, and S. A. Rodríguez. 2015. Mechanical Properties and Phases Determination of Low Carbon Steel Oxide Scales Formed at 1200°C in Air. *Surface and Coatings Technology*. 282: 155–162. Doi: 10.1016/j.surfcoat.2015.10.028.
[43] T. Amano *et al.* 2006. Hardness of Oxide Scales on Fe-Si Alloys at Room- and High-Temperatures. *MSF*. 522–523. 469–476. Doi: 10.4028/www.scientific.net/MSF.522-523.469.
[44] O.Barrau, C. Boher, C. Vergne, F. Rezai-Aria, and R. Gras. 2002. Investigations of Friction and Wear Mechanisms of Hot Forging Tool Steels. *International Tooling Conference*, France. 81–94.